

LETTER TO THE EDITOR

# High-resolution observations of the symbiotic system R Aqr

## Direct imaging of the gravitational effects of the secondary on the stellar wind

V. Bujarrabal<sup>1</sup>, J. Alcolea<sup>2</sup>, J. Mikołajewska<sup>3</sup>, A. Castro-Carrizo<sup>4</sup>, and S. Ramstedt<sup>5</sup>

<sup>1</sup> Observatorio Astronómico Nacional (OAN-IGN), Apartado 112, E-28803 Alcalá de Henares, Spain  
e-mail: v.bujarrabal@oan.es

<sup>2</sup> Observatorio Astronómico Nacional (OAN-IGN), C/ Alfonso XII, 3, E-28014 Madrid, Spain

<sup>3</sup> Nicolaus Copernicus Astronomical Center, Polish Academy of Sciences, ul. Bartycka 18, PL-00-716 Warsaw, Poland

<sup>4</sup> Institut de Radioastronomie Millimétrique, 300 rue de la Piscine, 38406, Saint Martin d'Hères, France

<sup>5</sup> Department of Physics and Astronomy, Uppsala University, Box 516, 75120 Uppsala, Sweden

submitted 13 June 2018, accepted 11 July 2018

### ABSTRACT

We have observed the symbiotic stellar system R Aqr, aiming to describe the gravitational interaction between the white dwarf (WD) and the wind from the Mira star, the key phenomenon driving the symbiotic activity and the formation of nebulae in such systems. We present high-resolution ALMA maps of the  $^{12}\text{CO}$  and  $^{13}\text{CO}$   $J=3-2$  lines, the 0.9 mm continuum distribution, and some high-excitation molecular lines in R Aqr. The maps, which have resolutions ranging between 40 milliarcsecond (mas) and less than 20 mas probe the circumstellar regions at suborbital scales as the distance between the stars is  $\sim 40$  mas. Our observations show the gravitational effects of the secondary on the stellar wind. The AGB star was identified in our maps from the continuum and molecular line data, and we estimated the probable position of the secondary from a new estimation of the orbital parameters. The (preliminary) comparison of our maps with theoretical predictions is surprisingly satisfactory and the main expected gravitational effects are directly mapped for the first time. We find a strong focusing in the equatorial plane of the resulting wind, which shows two plumes in opposite directions that have different velocities and very probably correspond to the expected double spiral due to the interaction. Our continuum maps show the very inner regions of the nascent bipolar jets, at scales of some AU. Continuum maps obtained with the highest resolution show the presence of a clump that very probably corresponds to the emission of the ionized surroundings of the WD and of a bridge of material joining both stars, which is likely material flowing from the AGB primary to the accretion disk around the WD secondary.

**Key words.** stars: AGB and post-AGB – circumstellar matter – binaries: close – binaries: symbiotic – stars: individual: R Aqr

### 1. Introduction

Symbiotic stellar systems (SSs) are interacting binaries consisting of an evolved cool giant and a compact companion, usually an AGB star and a white dwarf (WD). In classical SSs, the interaction is very strong; there are copious mass transfer, equatorial flows, and ejection of fast bipolar jets. The relevance in the SS activity of the gravitational interaction between the wind from the primary and the compact secondary is stressed in recent 3D simulations, see Mohamed & Podsiadlowski (2012), de Val-Borro et al. (2017), and Saladino et al. (2018). Those calculations revealed a new mass-transfer mode called wind Roche-lobe overflow (WRLOF), which happens when grains form in the AGB circumstellar envelope beyond the Roche lobe and the wind velocity is still moderate when it reaches the surroundings of the secondary, significantly reinforcing the companion-wind interaction. The resulting outflows are strongly focused toward the binary orbital plane and mass-transfer and accretion rates are at least an order of magnitude higher than previously predicted.

R Aqr is the best studied SS. The primary is a bright Mira-type variable and the companion is a WD. The two-arcminute-wide nebula is composed of an equatorial structure elongated in the east-west direction and a precessing jet (with position angle, PA, ranging between  $10^\circ$  and  $45^\circ$ ) powered by the accretion onto the WD; see Solf & Ulrich (1985), Melnikov et al. (2018),

and references therein. The orbital period of the binary system is long,  $\sim 43.6$  yr, and the orbital plane is roughly perpendicular to the plane of the sky and projected in the east-west direction (Gromadzki & Mikołajewska 2009). Recent Very Large Telescope (VLT) imaging by Schmid et al. (2017) resolved both stars, which were found to be separated by  $\sim 45$  milliarcsecond (mas). The photospheric diameter of the AGB star,  $\sim 10$ -20 mas, was measured from IR interferometry by Ragland et al. (2008) and Wittkowski et al. (2016). Molecular emission is very rarely observed in SSs, probably because of photodissociation by the UV emission of the WD and its surroundings or to strong disruption of the shells, except from regions very close to the AGB. However, R Aqr has been detected in SiO, H<sub>2</sub>O, and CO emission and is relatively well studied in molecular lines (Bujarrabal et al. 2010). Parallax measurements from SiO Very Long Baseline Interferometry (VLBI) data indicate a distance of 218 pc (Min et al. 2014), although the distance from the GAIA parallax is 320 pc; the origin of such a discrepancy is unknown. Both measurements are subject to uncertainties, because the stellar diameter is larger than the measured parallax and the SiO emission is still wider and less uniform than the stellar disk.

Predictions of WRLOF models agree with the observed large-scale nebular structure in SSs and the requirements to explain their activity. However, there is no direct observational information on how the gravitational effects of the secondary on

**Table 1.** Main line parameters derived for high-excitation lines and  $^{29}\text{SiO}$  absorption. We always give the R.A. and dec. offsets with respect to the total continuum centroid: 23:43:49.4962, -15:17:0.4.72.

molecular line	total flux mJy×km/s	peak brightness mJy/beam×km/s	$\Delta(\text{R.A.})$ mas	$\Delta(\text{dec})$ mas
$\text{H}_2\text{O } \nu_2=2 \ 3(2,1)-4(1,4)$	$370\pm 15$	$174\pm 7$	$11\pm 3$	$3\pm 3$
$\text{Si}^{17}\text{O } \nu=1 \ J=8-7$	$100\pm 6$	$53\pm 4$	$10\pm 3$	$2\pm 3$
$\text{CO } \nu=1 \ J=3-2$	$310\pm 7$	$132\pm 5$	$11\pm 3$	$3\pm 3$
$^{29}\text{SiO } \nu=0 \ J=8-7$ (abs.)	$-53\pm 4$	$-48\pm 4$	$9\pm 4$	$0\pm 4$
$\text{SO } ^3\Sigma \nu=1 \ 9(8)-8(7)$	$307\pm 8$	$130\pm 5$	$14\pm 3$	$5\pm 3$

the stellar wind take place. We present ALMA maps of radio continuum and molecular lines in R Aqr that show very clearly those effects at orbital and suborbital scales of  $\sim 10$ -40 mas.

## 2. Observations

Observations were performed with ALMA on November 21 and 23, 2017, for three tracks of 1.3 h each. Data were obtained with 47-48 antennas, with baselines ranging from 92 m to 8.5 km. The correlator was set to observe with four spectral windows, centered at frequencies 330583, 331295, 343495, and 345791 MHz, and with spectral resolutions 0.24, 0.98, 0.98 and 0.12 MHz, eventually smoothed in the final maps. The quasar J2348-1631 (1.6 away from R Aqr) was the phase calibrator, and J0006-0623 was the bandpass and flux calibrator: a flux reference of 1.58/1.65 Jy (at the lowest/highest frequencies) was adopted for the three tracks. Differences in the phase calibrator flux of 5% between consecutive tracks were found, which is a limit to the flux uncertainty. The data calibration was performed using the ALMA pipeline delivered with the CASA software.

For image cleaning, we used the Hogbom method and the Briggs weighting scheme with a robust value of 1, resulting in maps with half-power beam width (HPBW)  $\sim 40\times 35$  mas, see Figs. 1 and 3. The half-power field of view and the maximum recoverable scales are  $\sim 18''$  and  $\sim 2''$ , respectively. To better investigate the compact continuum clump, we also produced images of less sensitivity but higher spatial resolution using only data from baselines longer than 2.5 km and uniform weighting, which resulted in a beam of  $17\times 27$  mas. The distribution of the clean components (i.e. where the flux is deduced to come from) in this map was analyzed by means of a yet higher resolution image, by imposing a circular restoring beam of 10 mas (red contours in Fig. 2). See App. A for a more detailed description of our continuum mapping.

## 3. Results and conclusions

### 3.1. Summary of observational results

We have detected several molecular lines as well as the continuum emission at  $\lambda = 0.9$  mm from R Aqr. As mentioned, continuum maps were obtained weighting the visibilities in two different ways. Together with a more conservative standard procedure that leads to a resolution of about  $30\times 40$  mas, we also used a weighting that favors long baselines, leading to a resolution of  $\sim 10$ -20 mas. See Sect. 2 and Appendix A and Figs. 1 and 2. All our maps are centered on the continuum emission centroid (ICRS coordinates R.A.: 23:43:49.4962, dec.: -15:17:04.72), to which the offsets given in this letter always refer.

The maximum in the high-resolution continuum map is placed (with respect to the continuum emission centroid) at  $\Delta(\text{R.A.}) = +8$  and  $\Delta(\text{dec}) = -0.4$  mas; i.e. the continuum peak coordinates are ICRS R.A. 23:43:49.49657, dec. -15:17:04.7204.

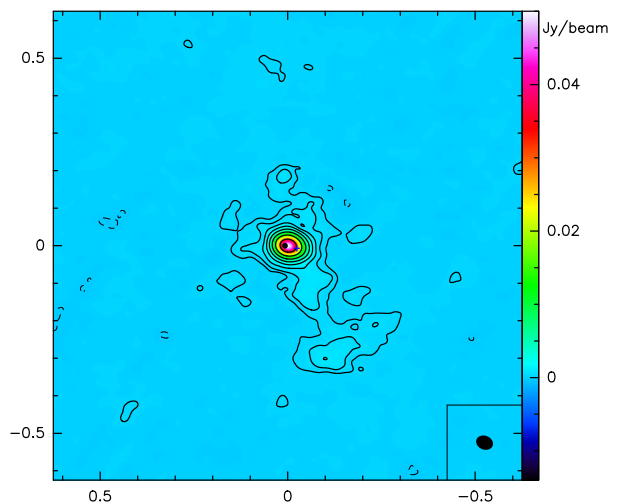


**Fig. 1.** ALMA map of the 0.9 mm continuum in R Aqr. The level spacing is logarithmic, with first contour at 0.25 mJy/beam and a jump of a factor 2; dashed contours represent negative values. The map center is the continuum centroid and the positions of the two stars are indicated. See the HPBW in the inset.

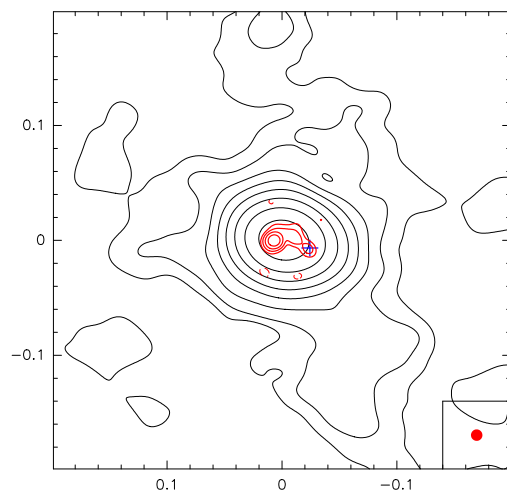


**Fig. 2.** High-resolution continuum map obtained using a 10 mas restoring beam (Sect. 2), red contours. The scale is logarithmic: the first contour is 1.5 mJy/beam and the jump is a factor 2; the dashed contours represent negative values. The expected position of the WD is shown with error bars (blue cross, see Sect. 3.2 and App. B); the Mira is coincident with the maximum of the high-resolution map. The central part of our standard continuum map (Fig. 1) is reproduced in black contours.

As we see in the following, that maximum is expected to represent the Mira position. By fitting in the  $uv$  plane a disk-like distribution, i.e. uniform and round, we find a 15-mas-wide disk with a center placed at +4.5 and 0 mas. In our case, the astrometry uncertainties are dominated by the phase stability (see the ALMA Cycle 5 Technical Handbook); we thus expect absolute errors  $\sim 3$  mas, which are sufficient for our purposes (Sect. 3.3). A smaller uncertainty, at least in relative positions, can probably be reached after a deeper data analysis.

We also detected several molecular lines: the intense  $^{12}\text{CO}$  and  $^{13}\text{CO } J=3-2$ , and, among the weaker lines,  $\text{H}_2\text{O } \nu_2=2 \ 3(2,1)-4(1,4)$  (331.123730 GHz),  $\text{Si}^{17}\text{O } \nu=1 \ J=8-7$  (332.021994 GHz),  $^{12}\text{CO } \nu=1 \ J=3-2$  (342.647636 GHz),  $^{29}\text{SiO } \nu=0 \ J=8-7$  (342.980847 GHz) and  $\text{SO } ^3\Sigma \nu=1 \ 9(8)-8(7)$  (343828.513 GHz). The  $^{29}\text{SiO } \nu=0$  line shows blueshifted absorption against the stellar continuum (in the range between  $-29 \text{ km s}^{-1}$  and  $-33 \text{ km s}^{-1}$

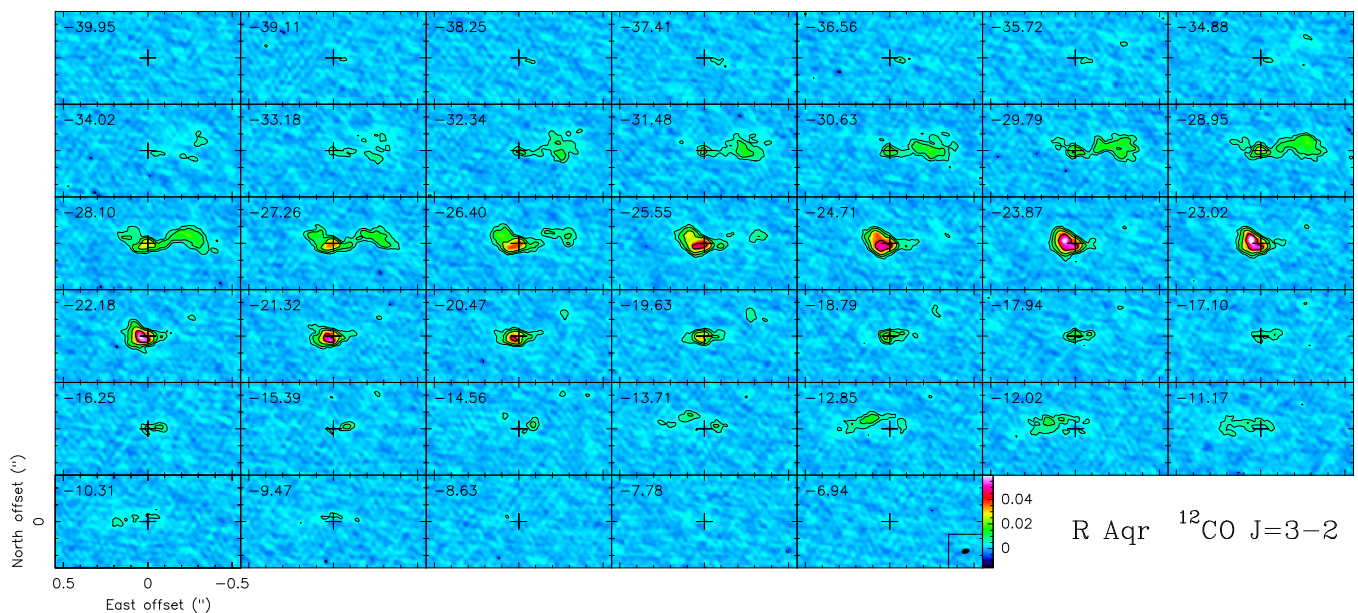


**Fig. 3.** ALMA maps per velocity channel of  $^{12}\text{CO } J=3-2$  emission in R Aqr; see the *LSR* velocities in the upper left corners. The center is the centroid of the continuum, whose image has been subtracted. The contours are logarithmic with a jump of a factor 2 and a first level of  $\pm 5$  mJy (equal to 6.2 times the rms and equivalent to 34.8 K); dashed contours represent negative values. The HPBW is shown in the inset, last panel.

*LSR*), very probably owing to gas in expansion in front of the star. The high-excitation ( $v > 0$ ) lines and the absorption feature show compact, barely resolved distributions. In Table 1, we give the main properties of those lines, including the centroids of their distributions, which are necessary to identify the AGB star (Sect. 3.2), and  $1\sigma$  uncertainties. Only the CO  $v=0$  lines, mainly the  $^{12}\text{CO}$  line, show a significant extent  $\geq 0''.5$  (Sect. 3.4). Recent ALMA maps by Ramstedt et al. (2018), which have a resolution of  $0''.5$ , detected clumps at  $\Delta(\text{R.A.}) \sim \pm 0''.8$ , also present in our maps but with a relatively poor signal-to-noise ratio (S/N).

### 3.2. Position of the binary system

The high-excitation lines detected in our data are expected to come from the close surroundings of the AGB star and to be good tracers of its position, as found from VLBI measurements of R Aqr and ALMA maps of other AGBs; see Min et al. (2014), Decin et al. (2018), etc. The absorption in the  $^{29}\text{SiO } v=0$   $J=8-7$  line must represent absorption by inner shells just in front of the star and should also be a very good tracer of its position. As we have seen, see Sect. 3.1 and Table 1, all our high-excitation lines and the  $^{29}\text{SiO } v=0$  absorption show indeed compact images, whose centroids are practically coincident within the uncertainties and given the extents of the observed distributions ( $\sim 35-55$  mas). Their positions can also be considered coincident with the continuum peak detected with the highest resolution (Sects. 3.1, 3.3); the coincidence between the  $^{29}\text{SiO}$  absorption and the continuum maximum is particularly good. The differences are significantly smaller than the expected diameter of the star,  $\sim 10-20$  mas. In any case, the line emission centroids tend to be shifted by about  $+3$  mas in R.A. with respect to the position obtained from the continuum (Sect. 3.1). It is difficult to discern which of the methods traces the Mira position more accurately: the measured continuum centers could be shifted westward, because of contamination from emission from the extended continuum or irradiation of the primary surface, and the line emission, even if it is compact, could be slightly shifted eastward because of the molecule emission suppression observed clearly in  $^{12}\text{CO}$  (Sect.

3.4). Needless to say, it is possible that the photospheric surface and nearby surroundings are not uniform, which would not allow comparisons at scales much smaller than  $\sim 10$  mas. We therefore conclude that the continuum peak position, namely ICRS R.A. 23:43:49.49657, dec.  $-15:17:04.7204$ , gives the AGB photosphere centroid with an accuracy of  $\pm 3$  mas. We have checked that these coordinates are fully compatible with the GAIA DR2 data. We recall that the AGB star position is in any case not coincident with the centroid of the total continuum emission (Sect. 2), which is taken as the center in all maps presented here.

As mentioned before, the two stars were imaged in 2014.9 by Schmid et al. (2017). Our ALMA observations were obtained three years later, and a moderate, but non-negligible change in the relative positions is expected. We estimated that change by adapting the orbital parameters determined by Gromadzki & Mikołajewska (2009) to the measurement by Schmidt et al. The derivation of the new orbit parameters is presented in App. B; we plan to widely discuss these in a future paper. Our conclusion is that in 2017 the secondary was placed at about  $-31$  mas in R.A. and  $-7$  mas in declination, with respect to the Mira star, with an uncertainty of about  $\pm 7$  mas; we note that the secondary is approaching us. The positions of both stars are shown in some of our figures.

### 3.3. Continuum 0.9 mm maps

Our 0.9 mm continuum map is shown in Fig. 1; the beam size at half maximum (FWHM) is  $\sim 30 \times 40$  mas. The expected positions of both stars are also given in Fig. 1. The AGB primary is represented by the black dot, whose width is roughly equal to the AGB photospheric disk, and the blue cross gives the position of the WD with the uncertainties; the stellar locations are discussed in the previous subsection and Apps. A, B. As we can see, the main continuum component is very compact, slightly elongated in the east-west direction, roughly in the direction of the apparent orbit shape (see App. B). In addition to the prominent maximum, there is a low-brightness component elongated in the direction of the large-scale jet (Sect. 1). This component is

very probably the base of the bipolar jets, which we detect down to scales of 30 mas, some AU. The total flux is  $\sim 100$  mJy, of which  $\sim 70$  mJy comes from the central condensation; this value is only somewhat larger than the expected flux coming from the primary photosphere,  $\sim 35$  mJy (for the photospheric size discussed in Sect. 1). The photosphere represents, therefore, an important component of the total continuum emission at 0.9 mm, with significant contributions from nearby stellar surroundings and the jet.

To better show the structure of the central continuum, we performed additional higher resolution maps, selecting only the longest baselines (Sects. 2, 3.2, and App. A; see results in Fig. 2). This procedure yields a very high resolution, but also a significant amount of lost flux and a worse S/N; this was possible only because of the very high dynamic range of the continuum observations. We can see that the jet is resolved out and only the intense compact component is recovered. This compact region is composed of a maximum placed on the expected AGB star position plus an extension in the direction of the companion (Sect. 3.2, Apps. A, B). Remarkably, there is a secondary clump almost exactly coincident with the WD position predicted from our new orbit determination (Sect. 3.2) and a third component joining both maxima. The intensity and spectral index of these components support our identifications (App. A). We think that this high-resolution continuum map is actually detecting both stars (or emission coming from their close surroundings) and the transfer of material from the primary to the secondary.

### 3.4. $^{12}\text{CO } J=3-2$ maps

$^{12}\text{CO}$  and  $^{13}\text{CO } J=3-2$  are the only lines that show a significant extent in our maps, particularly the  $^{12}\text{CO}$  line discussed here. The  $^{12}\text{CO}$  maps per velocity are shown in Fig. 3. In Fig. 4, we present the map of the velocity-integrated flux; the expected positions of the two stars are also shown, as derived in Sect. 3.2. We also show the position-velocity diagram found for a central cut in the east-west direction. In our maps, there is a compact central component plus two plumes of emitting gas at relatively negative and positive velocities, extending to the west and to the east, respectively, occupying in total about  $0''.7$  ( $\sim 200$  AU,  $3 \times 10^{15}$  cm). We note that the  $^{12}\text{CO } J=3-2$  maximum is not placed on the maximum found for the other lines (including  $^{13}\text{CO } J=3-2$ ) and for the continuum, but eastward by 20-30 mas. We suggest that this is due to the effects of photodissociation or shell disruption, which tend to suppress molecular line emission in SSs (Sect. 1) and must be more important in regions closer to the companion.

The emission distribution, extending in the east-west direction, is similar to the expected image of the two spiral arms predicted by WRLOF models; see for example Figs. 1, 2 and 3 of Mohamed & Podsiadlowski (2012), model M1 (in theoretical papers the velocity is often represented in a comoving frame). We recall that the orbit and equatorial planes are almost seen edge-on with the north pole slightly pointing toward us, the projected direction of the orbit is roughly in the east-west direction or slightly inclined ( $\text{PA} \gtrsim 90^\circ$ ), and the secondary is approaching us; see Sect. 3.2 and App. B. The CO structure, clearly elongated in the direction of the projected orbit, obviously corresponds to mass ejection strongly focused in the orbital plane. The shape and velocity of the plumes are similar to those expected for the projection in the plane of the sky of the spiral-like arms. The westward plume shows a negative velocity shift with respect to the systemic velocity of  $\sim -10$  km s $^{-1}$ , which is compatible with expectations: we know that the secondary is moving with velocities of this order (from the spectroscopic stellar data and stel-

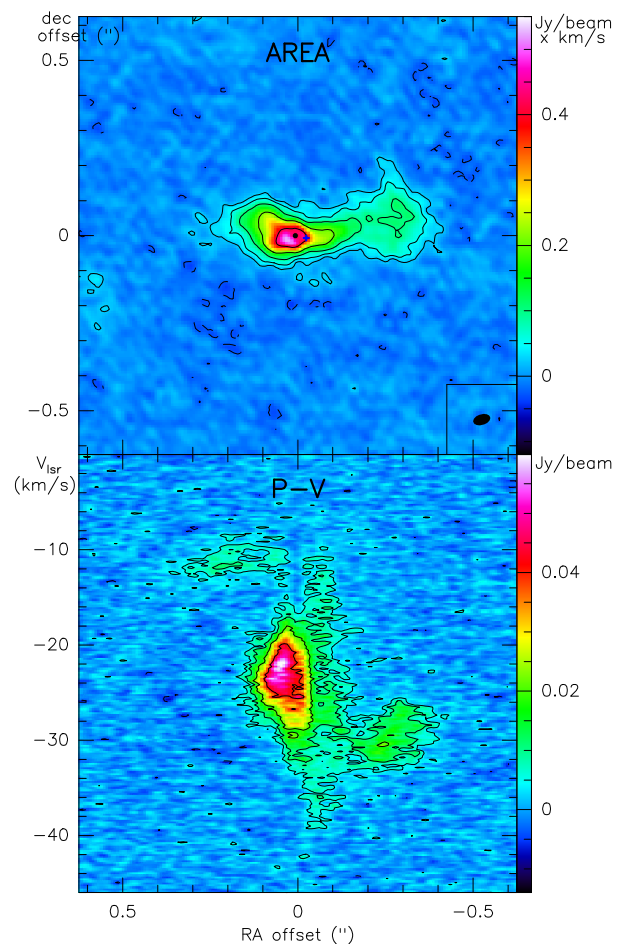


**Fig. 4.** *Top:* Map of the  $^{12}\text{CO } J=3-2$  velocity-integrated brightness in R Aqr. Contours are logarithmic, the first contour is  $\pm 0.025$  Jy/beam $\times$ km/s and the jump is a factor 2. Dashed contours represent negative values. *Bottom:* Position-velocity diagram for an east-west central cut.

lar dynamics in Gromadzki & Mikołajewska 2009) and that it efficiently drags the nearby gas (from hydrodynamical calculations). Up to a R.A. offset of  $-0''.2$ , it shows a slightly curved shape with concavity pointing northward, which is the expected projected shape of the inner spiral arm that is now being pushed by the companion. The outer clump at offset  $\sim -0''.3$  seems to represent the second spiral arm, which must also move toward us but at a slightly lower velocity. Finally, emission at relatively positive velocities (between  $-14$  and  $-9$  km s $^{-1}$  LSR, Figs. 3 and 4) mostly comes from a plume placed eastward and northward, exactly as expected for material accelerated by the passage of the secondary about half an orbit ago and that, therefore, moves away from us.

The whole set of molecular line data and a quantitative comparison with model predictions will be presented in a forthcoming paper. We think that our CO maps directly show the very strong gravitational effects of the WD secondary on the circumstellar wind leaving the AGB primary, including strong confinement to the equatorial plane and the formation of a double spiral extending significantly beyond the orbit.

*Acknowledgements.* This work has been supported by the Spanish MINECO, grant AYA2016-78994-P, and by the National Science Centre, Poland, grant OPUS 2017/27/B/ST9/01940. This paper makes use of the following ALMA data: ADS/JAO.ALMA#2017.1.00363.S. ALMA is a partnership of ESO (representing its member more states), NSF (USA) and NINS (Japan), together with NRC (Canada), MOST and ASIAA (Taiwan), and KASI (Republic of Korea), in

cooperation with the Republic of Chile. The Joint ALMA Observatory is operated by ESO, AUI/NRAO and NAOJ.

## References

- Balick, B., & Frank, A. 2002, *ARA&A*, 40, 439
- Bujarrabal, V., Mikołajewska, J., Alcolea, J., & Quintana-Lacaci, G. 2010, *A&A*, 516, A19
- Decin, L., Richards, A. M. S., Danilovich, T., Homan, W., & Nuth, J. A. 2018, arXiv:1801.09291
- de Val-Borro, M., Karovska, M., Sasselov, D. D., & Stone, J. M. 2017, *MNRAS*, 468, 3408
- Gromadzki, M., & Mikołajewska, J. 2009, *A&A*, 495, 931
- Hollis, J. M., Pedelty, J. A., & Lyon, R. G. 1997, *ApJ*, 482, L85
- Min, C., Matsumoto, N., Kim, M. K., et al. 2014, *PASJ*, 66, 38
- Melnikov, S., Stute, M., & Eisloffel, J. 2018, arXiv:1802.00503 (*A&A*, in press)
- Mohamed, S., & Podsiadlowski, P. 2012, *Baltic Astronomy*, 21, 88
- Ragland, S., Le Coroller, H., Pluzhnik, E., et al. 2008, *ApJ*, 679, 746-761
- Ramstedt, S., Mohamed, S., Olander, T., et al. 2018, *A&A*, in press
- Saladino, M. I., Pols, O. R., van der Helm, E., et al. 2018, arXiv:1805.03208
- Schmid, H. M., Bazzon, A., Milli, J., et al. 2017, *A&A*, 602, A53
- Solf, J., & Ulrich, H. 1985, *A&A*, 148, 274
- Wittkowski, M., Chiavassa, A., Freytag, B., et al. 2016, *A&A*, 587, A12

## Appendix A: High-resolution continuum maps

For the continuum images we only used the two spectral windows with the highest bandwidths in both receiver side-bands (centered at 331.295 and 343.495 GHz). The data were first mapped seeking for spectral lines that were flagged out. Line-free data from the two side-bands were combined and then imaged and cleaned using CASA. As mentioned, we first used a robustness factor of 1, which resulted in a clean/restoring beam of  $30 \times 40$  mas at PA  $69^\circ$  (Sect. 2, Fig. 1). To investigate the strong compact component, we also produced images using only data from baselines of 2.5 km length and above and adopting a robustness factor of  $-2$  (equivalent to uniform weighting). In this way we filter any contribution from structures with sizes  $\geq 70$  mas out, but reach a higher resolution. The final HPBW is  $17 \times 27$  mas (at PA  $51^\circ$ ), with an rms of  $220 \mu\text{Jy beam}^{-1}$ ; the resulting map is shown in Fig. A.1. The emission appears clearly resolved with a strong central component and a curved extension first to the west and then to the south; the jet emission is resolved out. The peak and total fluxes in this map are  $28 \text{ mJy beam}^{-1}$  and  $42 \text{ mJy}$  respectively; about 60% of the flux is recovered. Given our limited angular resolution, we analyzed the distribution of clean components (which represent where in our maps the emission is deduced to come from), by producing a yet higher resolution version of the map with a circular restoring beam of 10 mas HPBW (see Fig. 2). These procedures are often applied in radiointerferometry and are justified as far as the restoring beam is significantly larger than the clean beam size divided by the S/N or, more restrictively, divided by the intensity ratio of the significant clean components to those in adjacent regions. We have checked that the emission from, for instance, the southern, 10-mas wide area between the maxima outside the lowest level in Fig. B.1 is 10-30 times weaker than the maxima themselves. Continuum emission appears clearly separated in three locations: from left to right, components A, B, and C (Fig. B.1), which show peak (total) fluxes of 23 (31), 6 (10) and 5  $\text{mJy beam}^{-1}$  (5 mJy), respectively, and an rms of  $250 \mu\text{Jy beam}^{-1}$ . Comparing the fluxes obtained at 331 and 343 GHz separately, we estimated the spectral index of these three emitting spots; we found values of about 1.9, 3.1, and 1.0 for components A, B, and C, respectively.

Component A is coincident in position with the emission from vibrationally excited lines and the absorption feature of  $^{29}\text{SiO}$  (Sect. 3), suggesting that this is indeed the emission from the Mira component in the system. We checked that this position is also coincident within the uncertainties with the GAIA coordinates for R Aqr, which are expected to give the coordinates of the bright primary (after correcting for proper movements). Its total flux (31 mJy) and peak brightness are compatible with those expected from the Mira (for a temperature of  $\sim 2650$  K, Sect. 3) and its spectral index strongly suggests optically thick photospheric emission. We estimated the position of the WD companion for the epoch of our ALMA observations (2017.9), see Sect. 3 and App. B, which is found to be coincident with our C component within the errors. This coincidence and the measured spectral index, which is compatible with emission from the ionized surroundings of the WD, strongly suggest that this emission points to the location of the companion. Under the assumption that continuum components A and C identify the primary and the companion in R Aqr, then the intermediate component B, which shows a spectral index compatible with dust emission, would be the first detection of mass transfer between the stars in a SS.

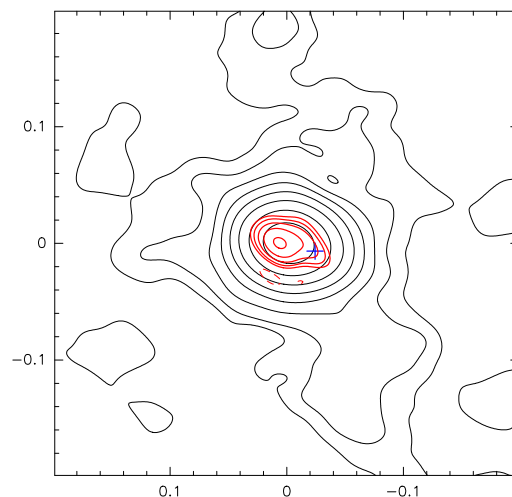


**Fig. A.1.** Same as Fig. 2, same scales and units, but showing the continuum map obtained after increasing the angular resolution and using the original clean beam ( $17 \times 27$  mas).

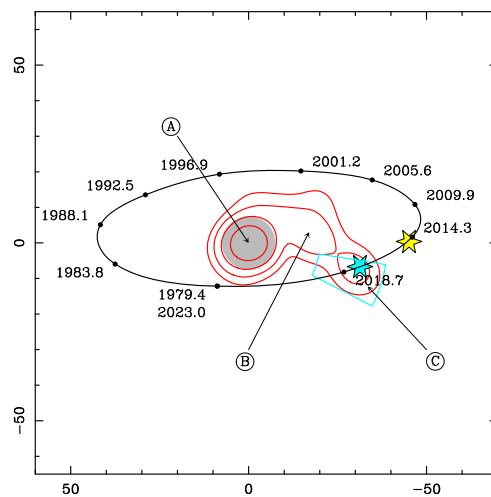


**Fig. B.1.** Relative movement of both stars (mas), according to the new orbital parameters. The AGB star is represented by the gray circle (with a diameter of 15 mas), the position of the WD in Schmid et al. (2017, epoch 2014.9) is indicated by the yellow asterisk, and the position of the WD derived from the new orbital parameters for the epoch of our observations (2017.9) is indicated by the blue asterisk. The uncertainties are represented by the blue contour. Small black dots show the position of the WD at orbital phases of 0.1 to 1.0 by 0.1 (the corresponding dates are also indicated). Our high-resolution continuum map is again shown (red contours) with the A, B, and C components; see App. A.

## Appendix B: New orbital parameters determined accounting for recent stellar astrometry

The determination of the orbital movements is fundamental to comparing the positions of the stars with the ALMA maps. Since the astrometric measurements by Schmid et al. (2017, VLT/SPHERE-ZIMPOL observations at epoch 2014.9), who relatively placed both stars with a reasonable accuracy, we can expect a small but noticeable change in the relative positions for 2017.9. The best determination of the orbital parameters of the R Aqr system is that by Gromadzki & Mikołajewska (2009). These authors derived the spectroscopic orbit from radial velocity measurements of the Mira, and used the resolved VLA observation of SiO masers and continuum emission at 7 mm by Hollis et al. (1997) to constrain the major axis and  $\Omega$ , the orientation of the

line of nodes on sky. Unfortunately, both results by Hollis et al. (1997) and Schmid et al. (2017) are not compatible: the results by Hollis et al. imply a large semimajor axis,  $a \sim 125$  mas, that is 2.7 times larger than the value resulting from data by Schmid et al. ( $a \sim 47$  mas), although both data predict similar values for  $\Omega$ ,  $\sim 90^\circ$  and  $93^\circ.5$ , respectively; we note that there was an error in the original number in Gromadzki & Mikołajewska (2009). The most likely explanation is that the claimed position for the WD in Hollis et al. (1997) is in fact an emission blow in the north jet. Indeed,  $H\alpha$  maps by Schmid et al. (2017) show bright jet knots near the central source. It is reasonable to assume that the WD at the epoch of the VLA observations by Hollis et al. (1997) was located somewhere between the two spots they detected, i.e., north of the Mira; the present stellar positions then indicate retrograde (clockwise) orbital motion.

In summary, we have recomputed the orbital parameters of the system in order to predict the relative position of the two stars at the epoch of our ALMA data, using the same radial velocity measurements as in Gromadzki & Mikołajewska (2009) and the relative position of the stars in Schmid et al. (2017). The new parameters are the same as in Gromadzki & Mikołajewska (2009), except for  $i$  (the inclination of the orbit w.r.t. the plane of the sky), which is now  $110^\circ$  (clockwise movement),  $\Omega$ , which is now  $93^\circ.5$ , and  $a$ , which is now 47 mas. The resulting new apparent orbit of the secondary and the prediction for the relative position of the two stars are shown in Fig. B1. We find that the distance between R Aqr B (the WD companion) and R Aqr A (the Mira primary) is  $32^{+7}_{-12}$  mas, at PA  $-102^{+3}_{-15}$ ; in our main discussion, the uncertainties are summarized by a single value of  $\sim \pm 7$  mas.

In a separate forthcoming paper we plan to discuss in detail the orbital parameters and improve their determination using data by Schmid et al. (2017), our ALMA measurements, and additional radial velocities from recent SiO maser data.